Published in final edited form as:
Cancer Immunol Res. 2015 February ; 3(2): 136–148. doi:10.1158/2326-6066.CIR-14-0036.

Tasquinimod modulates suppressive myeloid cells and enhances cancer immunotherapies in murine models

Li Shen[1,*], **Anette Sundstedt**[2,*], **Michael Ciesielski**[3], **Kiersten Marie Miles**[1], **Mona Celander**[2], **Remi Adelaiye**[1], **Ashley Orillion**[1], **Eric Ciamporcero**[1], **Swathi Ramakrishnan**[1], **Leigh Ellis**[1], **Robert Fenstermaker**[3], **Scott I. Abrams**[4], **Helena Eriksson**[2], **Tomas Leanderson**[2,5], **Anders Olsson**[2], and **Roberto Pili**[1]

[1]Genitourinary Program, Roswell Park Cancer Institute, Buffalo NY

[2]Active Biotech AB, Lund, Sweden

[3]Department of Neurosurgery, Roswell Park Cancer Institute, Buffalo, NY

[4]Department of Tumor Immunology, Roswell Park Cancer Institute, Buffalo, NY

[5]Immunology Group, Lund University, Lund, Sweden

Abstract

A major barrier for cancer immunotherapy is the presence of suppressive cell populations in cancer patients, such as myeloid-derived suppressor cells (MDSC) and tumor-associated macrophages (TAM), which contribute to the immunosuppressive microenvironment that promotes tumor growth and metastasis. Tasquinimod is a novel antitumor agent that is currently at an advanced stage of clinical development for treatment of castration-resistant prostate cancer. A target of tasquinimod is the inflammatory protein S100A9, which has been demonstrated to affect the accumulation and function of tumor-suppressive myeloid cells. Here, we report that tasquinimod provided a significant enhancement to the antitumor effects of two different immunotherapeutics in mouse models of cancer: a tumor vaccine (SurVaxM) for prostate cancer and a tumor-targeted superantigen (TTS) for melanoma. In the combination strategies, tasquinimod inhibited distinct MDSC populations and TAMs of the M2-polarized phenotype ($CD206^+$). $CD11b^+$ myeloid cells isolated from tumors of treated mice expressed lower levels of arginase-1 and higher levels of inducible nitric oxide synthase (iNOS), and were less immunosuppressive *ex vivo*, which translated into a significantly reduced tumor-promoting capacity *in vivo* when these cells were co-injected with tumor cells. Tumor-specific $CD8^+$ T cells were increased markedly in the circulation and in tumors. Furthermore, T-cell effector functions, including cell-mediated cytotoxicity and IFNγ production, were potentiated. Taken together, these data suggest that pharmacologic targeting of suppressive myeloid cells by tasquinimod induces therapeutic benefit and provide the rationale for clinical testing of tasquinimod in combination with cancer immunotherapies.

Corresponding authors: Anders Olsson Ph.D., Active Biotech AB, Lund, Sweden anders.olsson@activebiotech.com, Roberto Pili MD, Roswell Park Cancer Institute, University at Buffalo, Elm & Carlton Streets, Buffalo, NY, 14263-0001, Tel 716-845-3851, Fax 716-845-4620, Roberto.Pili@RoswellPark.org.
*These authors contributed equally.

Keywords

Tasquinimod; immunotherapy; S100A9; MDSCs; TAMs

Introduction

Immunotherapies have gained momentum in cancer therapeutics following the recent approvals of drugs for the treatment of prostate cancer and melanoma. Sipuleucel-T dendritic cell (DC) vaccine is now available for treatment of patients with asymptomatic or minimally symptomatic, metastatic, castration-resistant prostate cancer [1]. Clinical observations have indicated that melanoma is an immunogenic tumor [2], and extended survival data have led to the approval of immune checkpoint inhibitor ipilimumab for the treatment of metastatic melanoma [3]. However, despite these clinical advances, immunotherapies for these diseases and solid tumors in general, benefit only a subset of patients, as intrinsic or acquired tumor immune tolerance remains a major hurdle.

A significant barrier in vaccine therapy is the presence of immunosuppressive soluble and cellular components including myeloid-derived suppressor cells (MDSC) [4] and tumor-associated macrophages (TAM) [5], which are induced by tumor- and stroma-secreted inflammatory mediators [6-8]. MDSCs facilitate tumor progression by impairing T and NK cell activation [9] and by modulating angiogenesis. Preclinical data have suggested a role for MDSCs in suppressing T-cell responses and inducing tolerance against tumor-associated antigens (TAA) [9]. In addition, by secreting IL10 and TGFβ, MDSCs induce the accumulation of other immunosuppressive cell populations such as regulatory T cells (Treg) [10-12]. Similarly, the presence of TAMs in the tumor microenvironment (TME) may inhibit the immune response [13]. Taken together, there is strong evidence supporting that targeting immunosuppressive MDSCs and TAMs and modifying the TME can improve the efficacy of immunotherapy.

Tasquinimod, a quinoline-3-carboxyamide analog, is in clinical development for treatment of prostate cancer and other solid tumors. In a placebo-controlled, phase II randomized trial, tasquinimod doubled the median progression-free survival (PFS) period and prolonged survival of patients with metastatic, castration-resistant prostate cancer [14, 15]. A phase III clinical trial to test the effect of tasquinimod in the same patient population is ongoing (NCT01234311). Tasquinimod has been shown to inhibit prostate cancer growth and metastasis in animal models [16-18]. Results from these studies have suggested that the anti-angiogenic property of this molecule may be responsible for its antitumor activity, since tumor growth inhibition was associated with reduced microvasculature density, increased expression and secretion of the angiogenesis inhibitor thrombospondin-1 (TSP-1), and down-regulation of VEGF and HIF-1α [19-20]. More recent data have suggested that tasquinimod may affect HIF by interfering with histone deacetylase 4 (HDAC 4) [21]. However, in an orthotopic, metastatic prostate cancer model, tasquinimod reduced the metastatic rate without affecting microvessel density in the primary tumor [18]. Therefore, mechanisms other than impairing angiogenesis may play an important role in the antitumor and anti-metastasis activities of tasquinimod.

S100A9, a Ca^{2+}-binding inflammatory protein, has been identified as a potential target of tasquinimod. S100A9 interacts with pro-inflammatory receptors Toll-like receptor 4 (TLR4) and receptor of advanced glycation end products (RAGE), and this interaction is inhibited by the specific binding of tasquinimod to S100A9 [22-23]. These receptors are expressed on the surface of multiple myeloid-cell populations, including MDSCs, macrophages, DCs, as well as endothelial cells. Functionally, S100A9 regulates the accumulation of MDSCs and inhibits DC differentiation [24] [25], which may lead to suppression of immune responses and tumor progression. Therefore, by targeting S100A9, tasquinimod has immunomodulatory activity and the potential to regulate multiple myeloid populations.

In this study, we tested the effect of tasquinimod on immunosuppressive myeloid-cell populations and investigated its immunomodulatory activity. We conducted preclinical studies of tasquinimod in combination with two different immunotherapeutic approaches in mouse models of prostate cancer and melanoma. Our results suggest that treatment with tasquinimod affects the tumor microenvironment by modulating suppressive myeloid-cell populations, leading to augmented immune responses and enhanced antitumor effects of immunotherapies.

Materials and Methods

Tumor cells

The development of castration-resistant (CR) Myc-CaP cell line has been reported previously [26]. CR Myc-CaP cell line was cultured in DMEM (Mediatech, Inc.) with 10% FBS. The 5T4-tranfected murine B16-F10 melanoma cell line (B16-h5T4) [27] was kindly provided by Peter Stern (Paterson Institute for Cancer Research, Manchester, UK) and was cultured in R10 medium (RPMI-1640 with Ultra glutamine (BioWhittaker/Lonza, Wokingham, UK); supplemented with 10% fetal bovine serum (Fisher Scientific, Pittsburgh, PA), 1 mM sodium pyruvate, 10 mM HEPES, 0.1 mg/ml gentamicine sulfate and 50 μM β-mercaptoethanol). The CR Myc-CaP and B16-h5T4 cell lines were tested to be mycoplasma-free; no other authentication assay was performed.

In vivo tumor growth

The animal protocols were approved by the Institutional Animal Care and Use Committee at Roswell Park Cancer Institute (protocol 1137 M), or by the Bioethics Committee in Lund, Sweden (M60-10), as indicated, and were in accordance with the NIH Guide for the Care and Use of Laboratory Animals. 1×10^6 CR Myc-CaP cells were inoculated subcutaneously in the right flank of castrated male FVB mice. Animals were distributed randomly into four treatment groups (7–9 animals/group): vehicle, vaccine (SurVaxM), tasquinimod (10 mg/kg/day in drinking water), or the combination. Mice were given 100 μg of SurVaxM peptide and 100 ng of GM-CSF by subcutaneous (s.c.) injection, once per week. The tumor size was measured by a caliper twice a week. At the end of the 3–4 week experiment, tumors and spleens were collected and analyzed. B16-h5T4 cells were cultured as described above, counted, re-suspended and maintained in iced-cold matrigel (BD Biosciences, San Jose, CA) at a concentration of 0.3×10^5 cells/ml. Tumor cells were implanted s.c. into the hind flank of C57Bl/6 mice on day 0 in a volume of 0.1 ml matrigel. Mice were treated with

tasquinimod (30 mg/kg/day in drinking water) either from day 0 or day 1 after tumor inoculation and throughout the experiments. For TTS treatment, mice were given daily injections of 5T4Fab-SEA (25 μg/kg) on days 3 to 6, or on days 9 to 11 for analysis of TTS-reactive T cells in the tumors. Experiments were terminated between day 16 and day 21. Tumor sizes were measured twice a week and tumor volumes were calculated as volume = $L \times W^2 \times 0.4$, where L is the length (mm) and W (mm) is the width of the tumor (L>W) [28]. Animal experiments and correlative studies in the CR Myc-CaP and the B16-h5T4 models were conducted at Roswell Park Cancer Institute and Active Biotech, respectively.

Splenocytes and tumor suspension preparation

For isolation of splenocytes, spleens were harvested, mashed on, and passed through a 70 μm strainer. These cell suspensions were centrifuged at 300 g for 10 min at 4°C. Cell pellets were treated with ACK lysing buffer (Biosource). Splenocytes were then resuspended and cultured in complete media (RPMI supplemented with 10% FBS, 1 mM sodium pyruvate, 100 mM non-essential amino acid, 2 mM L-glutamine, Pen (100 units/ml)-Strep (100 mg/ml) and 55 μM β-mecaptoethanol). Single-cell suspensions were prepared from tumors with mouse tumor dissociation kit (Miltenyi Biotech). Briefly, tumors were cut into small pieces and incubated in an enzyme-cocktail solution for 40 minutes at 37°C with agitation, followed by meshing the tumors in a 70 μm cell strainer. Alternatively, the tumors were cut into small pieces and incubated in 0.5 mg/ml Collagenase IV (Worthington Biochemical Corporation, Lakewood, NJ) and 0.1% DNase (Sigma-Aldrich, St. Louis, MO) for 45 min at 37°C, followed by meshing the tumors in a 70 μm cell strainer.

Cell staining and flow cytometry

Splenocytes, tumor single-cell suspensions, or peripheral blood cells were washed with flow buffer (PBS with 1% of FBS and 2 mmol/L of EDTA), then incubated with an Fc-blocking antibody (anti-mouse CD16/ CD32 mAb 2.4G2; BD Biosciences) and stained with fluorescence-conjugated antibodies against surface markers. Cells were then fixed in Fix/ Perm buffer (eBioscience) and stained with antibodies against intracellular proteins. The following fluorochrome-labeled antibodies were used: Gr1 (clone RB6-8C5), CD11b (clone M1/70), Ly6G (clone 1A8), Ly6C (clone AL-21), F4/80 (clone BM8), CD206 (clone C068C2), Arg 1 (polyclonal antibody, R & D systems®, Cat: IC5868A), iNOS (clone CXNFT), CD4 (clone RM4-5), CD8a (clone 53-6.7), TCR-Vβ3 (clone KJ25), and TCR-Vβ8 (clone F23.1) were purchased from BD Biosciences (San Jose, CA), eBioscience (San Diego, CA), BioLegend (San Diego, CA), and R & D systems. Cells stained with specific antibodies, as well as isotype-control stained cells, were assayed on a FACScalibur, a FACSCantoII, or a LSR II flow cytometer (BD Biosciences). Data analysis was performed using the FCS Express (De Novo Software) or FACS Diva software (BD Biosciences).

IFNγ induction assay

1×10^6 splenocytes were cultured with stimulation of PMA (Sigma, 20 ng/ml) and Ionomycin (Sigma, 1 μg/ml) for 5 hours. Brefeldin A (Sigma) was added to the cultures to block protein secretion. Cells were harvested and stained for surface markers, then fixed and stained for intracellular IFNγ (eBioscience) and analyzed by flow cytometry.

Granzyme B induction assay

1×10^6 splenocytes were cultured with stimulation of CD3 (eBioscience, 1 μg/ml) and CD28 (0.5 μg/ml) for 72 hours. Brefeldin A (Sigma) was added to the cultures during the last 5 hours of culture to block protein secretion. Cells were harvested and stained for surface markers, then fixed and stained for intracellular Granzyme B (eBioscience) and analyzed by flow cytometry.

T-cell suppression assays

1×10^5 T cells (isolated with a Pan T cell isolation kit, Miltenyi Biotec) were cultured in plates coated with CD3 (eBioscience, 1 μg/ml) and CD28 (0.5 μg/ml) for 72 hours. Different numbers of magnetic beads-purified $CD11b^+$ cells from tumors were added to the culture at the beginning. 1 μCi of ^{3}H-thymidine was added to the culture for the last 12 hours. Cells were then harvested and the incorporated ^{3}H-thymidine was detected with scintillation counting. Alternatively, $CD11b^+$ cells were added to CFSE-(Vybrant® CFDA SE Cell Tracer Kit; Molecular Probes) labeled T cells (isolated from naïve spleens using a Pan T cell isolation kit from Miltenyi Biotec) activated by anti-CD3/anti-CD28 coated beads (Dynabeads®, Dynal) and incubated for 72 hours. The frequencies of divided $CD4^+$ and $CD8^+$ T cells were determined by FACS analysis.

Splenocyte- and CD8 T cell-mediated cytotoxicity assay

Cytotoxicity assay was performed by using Live/dead® cell-mediated cytotoxicity kit (invitrogen). CR Myc-CaP cells were labeled with Dio and cultured in complete medium. Splenocytes or isolated $CD8^+$ T cells were added to the culture in different ratios to tumor cells. After a 5-hour incubation, all cells in culture were harvested and PI staining was performed to detect dead cells. Cell cytotoxicity was analyzed by calculating percentage of dead cells with Dio label compared to the whole cell population with Dio label. Cell events were acquired using LSRII and FACSDiva. Data were analyzed with FCS Express (De Novo Software).

Antigen-specific tetramer binding assay

Blood samples (100 μl) and splenocytes (1×10^6 cells) were incubated for 30 minutes with 10 μl of iTAg MHC Class I Murine H2-K^b Tetramer-SA-PE bound by MFFCFKEL peptide with specificity for SurVaxM (Beckman Coulter) or iTAg MHC Class I Murine H2-K^b Tetramer-SA-PE bound by SIINFEKL ovalbumin peptide to represent negative control (Beckman Coulter). Samples were also labeled with 10 μl anti-CD8-FITC (clone 53.6.7; BioLegend). Following incubation, 1 ml of iTAg MHC Tetramer Lyse Reagent (Beckman Coulter) supplemented with 25 μl iTAg MHC Tetramer Fix Reagent (Beckman Coulter) was added to the samples, which were then incubated for 10 minutes at room temperature, subsequently washed with PBS, and resuspended in 400 μl of FluoroFix Buffer (BioLegend).

Immunofluorescence staining of tumor sections

Snap frozen tumors sliced into 8μm frozen sections and fixed in cold acetone for 10 min, before fluorescence labeling. Primary antibody, rat anti-mouse CD31 (BD, Mec 13.3;

1:1000) and secondary antibody, goat anti-rat alexa fluor 555 (Invitrogen, AF555; 1:500) in PBS (5% & 2% mouse serum respectively) were used, and slides were washed in PBS and mounted with fluorescence mounting medium (Dako, S3023). The sections were analyzed in a Leica DMRX-E microscope. Representative photos were taken and the density of CD31-positive cells (fluorescence) was measured with Leica QWin image analysis system.

Immunohistochemistry staining

Tissue specimens were fixed for 24-hr, paraffin embedded and 4μm sections were prepared. Sections were de-paraffinized and rehydrated through graded alcohol washes. Antigen unmasking was achieved by boiling slides in sodium citrate buffer (pH=6.0). Sections were further incubated in hydrogen peroxide to reduce endogenous activity. Then tissue section were blocked with 2.5% horse serum (Vector Laboratories) and incubated overnight in primary antibodies against CD31 (1:100, Dianova). Following anti-CD31 incubation, tissue sections were incubated in horseradish-conjugated anti-rat antibody according to manufacturer's protocol (Vector Laboratories) followed by enzymatic development in diaminobenzidine (DAB) and counter-stained in hematoxyline. Section were dehydrated and mounted with cytoseal 60 (Thermo Scientific). Corresponding isotype negative controls were used for evaluation of specific staining. Stained sections were analyzed under bright field using the Zeiss Axio microscope. The number of positive cells was determined in a blinded fashion by analyzing four random 20x fields per tissue and quantified using Image J software.

Quantitative Real-time PCR (qRT-PCR)

mRNA was extracted from $CD11b^+$ cells that were isolated as anti-$CD11b^+$ magnetic bead fractions from single-cell suspensions B16-h5T4 tumors. mRNA extraction was performed using the RNeasy mini kit (Qiagen, Hilden, Germany) and RNA concentration and purity was determined through measurement of A260/A280 ratios with a NanoDrop ND-1000 spectrophotometer. cDNA was prepared using the iScript kit (BioRad, Hercules, CA, USA) and qPCR was performed using a CFX384 real time PCR detection system (BioRad) with a three-step PCR-protocol (95°C for 10 min, followed by 45 cycles of 95°C for 10 sec and 58°C for 30 sec) using SYBR Green (SsoFast EvaGreen; BioRad) as fluorophore and expression levels were calculated (CFX Manager software; BioRad) as normalized ΔC_t expression values between the target gene and the two "housekeeping" genes β-Actin and Ywhaz. Data were presented as fold-induction ($2^{\Delta\Delta Ct}$) levels of treated tumors compared to control tumors (ΔΔCt). The primers used for target genes were: β-Actin_fw 5'- ATG CTC CCC GGG CTG TAT-3', β-Actin_rew 5'- CAT AGG AGT CCT TCT GAC CCA TTC -3', Ywhaz_fw AAC AGC TTT CGA TGA AGC CAT¸ Ywhaz_rew TGG GTA TCC GAT GTC CAC AAT, CD206_fw GCA AAT GGA GCC GTC TGT GC, CD206_rew CTC GTG GAT CTC CGT GAC AC, Arg-1_f w GTG AAG AAC CCA CGG TCT GT, Arg-1_rew CTG GTT GTC AGG GGA GTG TT, iNos_fw TGG TGG TGA CAA GCA CAT TT, iNos_rew AAG GCC AAA CAC AGC ATA CC, Cxcl9_fw TCA ACA AAA GAG CTG CCA AA, Cxcl9_rew GCA GAG GCC AGA AGA GAG AA, CxCl10_fw TCTGAGTCCTCGCTCAAGTG, CxCl10_rew CCTTGGGAAGATGGTGGTTA, Cxcl11_fw TCC TTT CCC CAA ATA TCA CG, Cxcl11_rew CAG CCA TCC CTA CCA TTC AT, Ccr2_fw ACT TTT CCG AAG GAC CGT CT, Ccr2_rew GTA ACA GCA TCC

GCC AGT TT, Ccl2_fw CAGGTCCCTGTCATGCTTCT, Ccl2_rew GTCAGCACAGAC CTCTCTCT. S100A9_fw CAG CAT AAC CAC CAT CAT CG, S100A9_rew GCC AAC TGT GCT TCC ACC AT, S100A8_fw GCT CCG TCT TCA AGA CAT CGT, S100A8_rew GGC TGT CTT TGT GAG ATG CC, IL-12b_fw GAAAGACCCTGACCATCACT, and IL-12b_rew CCTTCTCTGCAGACAGAGAC.

Nitric oxide synthase activity assay

The assay was performed with an ultra sensitive assay for nitric oxide synthase from Oxford Biomedical Research (Cat: NB78). Briefly, lysates from isolated CD11b cells were first incubated with substrates and cofactors. Then the mixtures were incubated with nitrate reductase to transform nitrate to nitrite, and mixed with coloring reagent to quantify total end-product concentration. These reactions were performed in a 96-well plate and absorbance was read at 540nm.

Statistical analysis

The difference in tumor weight between treatment groups was statistically evaluated by non-parametric Mann-Whitney U test. Differences between experimental groups were tested by either Student's t test or for variances by ANOVA. $P<0.05$ was considered statistically significant.

Results

Tasquinimod enhances the effect of immunotherapy in castration-resistant prostate cancer and melanoma models

Results from previous studies in experimental tumor models indicated that immunomodulatory effects of tasquinimod may contribute to its antitumor activity [23]. To investigate the potential immunomodulatory activities of tasquinimod, we tested this agent in combination with a survivin peptide vaccine (SurVaxM) in survivin-expressing CR Myc-CaP prostate cancer model and with a tumor-targeted superantigen in a B16 melanoma model.

Survivin is an intracellular TAA expressed in several solid tumors, including prostate cancer [29]. SurVaxM is a modified survivin peptide vaccine SVN53-67/M57-KLH [30] that we have tested previously in multiple tumor models [31]. FVB mice were inoculated with CR Myc-CaP cells subcutaneously. Tumor-bearing mice were divided into four groups and treated with vehicle, SurVaxM (1 dose/wk), tasquinimod (10 mg/kg/day in drinking water), or the combination of SurVaxM and tasquinimod. In the CR Myc-CaP model, SurVaxM and tasquinimod single treatments displayed modest antitumor effect but did not induce significant change in tumor growth (Fig. 1A, left panel). However, the combination of SurVaxM and tasquinimod significantly inhibited tumor growth (58% reduction, combination vs. vehicle, $p= 0.0002$). The combination treatment also significantly inhibited tumor growth compared to that of single treatment groups (tasquinimod vs. combination $p= 0.009$; survivin vs. combination $p= 0.017$). Similarly, both SurVaxM and tasquinimod single treatments induced modest but not significant reductions of tumor weight at the endpoint of

the study, while the combination induced more than additive effect, a 65% reduction from vehicle level (Fig. 1A, right panel, vehicle vs. combination, $p = 0.0002$).

In parallel, we tested tasquinimod in combination with a different immunotherapy approach, tumor-targeted superantigens (TTS) in a transplantable B16 melanoma model. TTS immunotherapy activates and directs T lymphocytes to attack tumor cells by means of fusion proteins between bacterial superantigens, such as staphylococcal enterotoxin A (SEA), and Fab-fragments of tumor-reactive monoclonal antibodies (mAb) [32]. Superantigens activate a high number of $CD4^+$ and $CD8^+$ T cells expressing particular T-cell receptor (TCR)-Vβ chains [33]. In this study, B16-h5T4-expressing tumors were treated with tasquinimod (30 mg/kg/day in drinking water), the TTS fusion protein 5T4Fab-SEA at a sub-optimal therapeutic dose (25 μg/kg), or the combination. Tasquinimod treatment began the day after tumor-cell inoculation and 5T4Fab-SEA was administrated on days 3-6. While both TTS and tasquinimod single-agent treatments elicited substantial antitumor effects, the combination regimen led to a significant reduction in tumor size at the endpoint (>75% reduction, vehicle vs. combination $p<0.0001$; Fig. 1B). Thus the combination of tasquinimod with two different immunotherapeutic strategies resulted in a significant enhancement of antitumor effects.

Enhanced immunotherapy elicited by tasquinimod combination is associated with induction of T-effector cells and increased antitumor immune responses

To determine whether the observed inhibition of tumor growth induced by the combination strategy was associated with improved immune responses, we examined $CD8^+$ T cells harvested at the end of the experiment. First, using a survivin vaccine-specific peptide-MHC class I tetramer binding assay we showed that the survivin vaccine, as a single treatment or in combination with tasquinimod, induced antigen-specific $CD8^+$ T cells (Supplementary Fig. 1). We also tested the cellular expression of IFNγ and Granzyme B, which are critical for $CD8^+$ T-cell effector functions. Splenocytes were isolated from differentially treated mice, stimulated and then stained for cell-surface markers and intracellular proteins. IFNγ expression was increased slightly in $CD8^+$ T cells from combination-treated animals as compared to vehicle group (Fig. 2A), while no significant changes were observed in $CD8^+$ T cells from single agent-treated animals. Similarly, when compared to vehicle- and single agent-treated groups, Granzyme B expression in $CD8^+$ T cells from combination-treated animals was significantly higher (Fig. 2B).

To determine whether the changes in specific $CD8^+$ T cells were associated with an improvement of cytotoxic T lymphocyte (CTL) activity, we tested *ex vivo* the ability of splenocytes and purified $CD8^+$ T cells to kill CR Myc-CaP tumor cells. Consistent with enhanced antitumor activity observed following combination treatment, splenocytes from these mice displayed significantly improved tumor-cell killing capacity as compared to those from other treatment groups (Fig. 2C, left panel). Interestingly, when purified $CD8^+$ T cells were used *ex vivo* in the same assay, tumor-cell killing capacity was equal in all treatment groups (Fig. 2C, right panel). Thus, these results suggest that the combination therapy does not enhance CTL activity *per se* but rather inhibits T cell-suppressing factor(s) in the cultured splenocytes.

In the B16-h5T4 melanoma model, analysis of tumor-infiltrating cells showed that the combination treatment significantly increased accumulation of $CD4^+$ and $CD8^+$ T cells measured at the endpoint as compared to those of control and single-agent treatments (Fig. 2D). To address the influence of tasquinimod on the activation of TTS-reactive T cells, B16-h5T4 tumors were allowed to grow until day 9 before giving 3 daily injections of 5T4Fab-SEA. Tumor-infiltrating cells were analyzed at different days (day 12-16) to follow the kinetics of specific T-cell expansion. Tasquinimod significantly enhanced and prolonged tumor-infiltration of TTS-reactive TCR-$V\beta3^+CD8^+$ T cells induced by 5T4Fab-SEA (Fig. 2E). The TTS-non-reactive TCR-$V\beta8^+CD8^+$ T cells were only marginally affected by the treatment (Fig. 2F). In contrast, the TCR-$V\beta3^+CD4^+$ T-cell population was less enhanced by the combination (Fig. 2G).

Tasquinimod has been reported to display anti-angiogenic activity in prostate cancer models [19, 34]. To determine whether the anti-angiogenic effect of tasquinimod was involved in enhancing the antitumor effects of immunotherapy, we assessed the microvasculature density (CD31 expression) in the harvested tumor tissue by either immunofluorescence or immunohistochemistry analysis in the two therapeutic strategies, respectively. The results showed that tasquinimod treatment reduced microvasculature density in B16 tumors (Fig. 3A), but it did not change tumor vasculature in the CR Myc-CaP model (Fig. 3B). In summary, these results suggest that the immunomodulatory effects of tasquinimod may be dissociated from its anti-angiogenic activity; and in the B16-h5T4 tumor model, the tasquinimod-induced inhibition of tumor blood vessel formation, may account at least in part for its antitumor effect in this model.

Infiltration of suppressive myeloid-cell populations is reduced by tasquinimod treatment in immunotherapy

S100A9 is an inflammatory protein that affects the accumulation of immunosuppressive myeloid cells, including MDSCs [24] [25]. Tasquinimod binds to S100A9, inhibiting its downstream signaling, and thus has the potential to affect myeloid cells. To investigate the mechanism of immune-promoting activity of tasquinimod in combination with immunotherapy, we analyzed the peripheral and tumor-infiltrating myeloid-cell populations.

In the CR Myc-CaP tumor model, blood samples were taken from differentially treated mice after two weeks of treatments and subjected to immunofluorescence staining and FACS analysis. We observed three different $CD11b^+$ cell populations in the blood distinct by their expression levels of the Gr1 marker; $Gr1^{negative}$, $Gr1^{low}$ and $Gr1^{high}$ (Supplementary Fig. 2A). Tasquinimod did not affect the number of either $Gr1^{low}CD11b^+$ cells or $Gr1^{high}CD11b^+$ MDSCs in the blood, but decreased the $Gr1^-CD11b^+$ population (Supplementary Fig. 2A). Similarly, MDSC number in the spleen did not change following treatments (Supplementary Fig. 2C). In addition, tumors were harvested from differentially treated mice and processed into suspension. Interestingly, tasquinimod significantly reduced the number of tumor-infiltrating MDSCs when given as a single agent or in combination with the vaccine (Fig. 4A). Further analysis of MDSC subpopulations present in the blood and tumors revealed a striking dominance of the granulocytic $CD11b^+Ly6C^{low}Ly6G^+$ population (Supplementary Fig. 2B and D).

Similar analysis of $CD11b^+$ cells and MDSC subpopulations was performed in the B16-h5T4 model (C57Bl/6 strain). The frequency of tumor-infiltrating $CD11b^+$ cells was not altered following tasquinimod treatment (Supplementary Fig. 3A), whereas a significant reduction of the number of $CD11b^+$ cells was observed in the spleen (Supplementary Fig. 3B). In contrast to that observed in the CR Myc-CaP model, the majority of MDSCs in untreated B16-h5T4 tumors was of the $CD11b^+Ly6C^{high}Ly6G^-$ monocytic subtype (Fig. 4B, left plot). Moreover, a significant reduction of the $CD11b^+Ly6C^{high}Ly6G^-$ monocytic subpopulation was observed while the proportion of $CD11b^+Ly6C^{low}Ly6G^+$ granulocytic MDSCs increased in tumors upon tasquinimod treatment (Fig. 4B). A comparable picture was also seen in the spleen (Supplementary Fig. 3C). Interestingly, the tumor-infiltrating $CD11b^+Ly6C^{high}Ly6G^-$ MDSCs expressed high levels of the angiopoietin receptor Tie2 (data not shown), which plays a key role in tumor angiogenesis [35]. Thus, the decrease in microvasculature density by tasquinimod in the B16 model could be the consequence of reducing pro-angiogenic monocytic cells within the tumors.

Tumor-associated macrophages are important components of the immunosuppressive TME. Immature monocytes and monocytic MDSCs migrate to the tumor in response to inflammatory mediators released from the TME. When infiltrating the tumor tissue, these cells adapt to the environment and differentiate into TAMs by losing Gr1 marker expression and gaining an even more immunosuppressive M2 macrophage phenotype [36] [37] [38]. Therefore, we assessed the effect of tasquinimod on TAMs. Results from the CR Myc-CaP model showed that tasquinimod treatment led to a reduction of infiltrating $CD206^+$ M2 TAMs (Fig. 4C). Similarly, analysis of macrophages in B16-h5T4 tumors also revealed a strong reduction of this subpopulation in tasquinimod-treated mice (Fig. 4D).

In addition to MDSCs and TAMs, we also investigated whether tasquinimod treatment affects immune-promoting activities of other myeloid and lymphoid cells. Tasquinimod did not impair T-cell expansion upon activation either in T cells isolated from differentially treated mice (Supplementary Fig. 4A), or when tasquinimod was added in culture (Supplementary Fig. 4B). Tregs represent an immunosuppressive lymphocyte population whose accumulation can be regulated by MDSCs. In both CR Myc-CaP (Supplementary Fig. 4C, left panel) and B16-h5T4 (Supplementary Fig. 4C, right panel) models, tasquinimod increased the accumulation of Tregs. DC differentiation has been shown to be regulated by the S100A9 protein [24]. Although tasquinimod slightly reduced the number of DCs in the spleen (Supplementary Fig. 5A), drug treatment did not impair the capacity of DCs to stimulate T cells (Supplementary Fig. 5B). These data suggest that immunosuppressive myeloid cells, such as MDSCs and TAMs but not other myeloid or lymphoid populations are the potential cellular targets of tasquinimod and they may be responsible for the immune-promoting activity of tasquinimod in combination with immunotherapies.

Tasquinimod inhibits immunosuppressive functions of tumor-associated myeloid cells and modulates relevant gene expression

So far, we have shown that tasquinimod significantly reduced the numbers of distinct MDSCs and altered the TAM populations in two different tumor models, suggesting that

tasquinimod may affect the accumulation/trafficking of immunosuppressive myeloid cells into the tumors. To investigate the mechanisms by which tasquinimod regulate these cells, we measured the immunosuppressive capacity of intratumoral $CD11b^+$ myeloid cells on T-cell activation. $CD11b^+$ cells were purified from tumor tissue and cultured with purified, stimulated T cells. As expected, $CD11b^+$ cells from tumors inhibited T-cell proliferation (Fig. 5A). However, $CD11b^+$ cells isolated from tasquinimod-treated CR Myc-CaP tumors showed significantly less suppression on T-cell proliferation compared to that of the controls (Fig. 5A). Similarly, $CD11b^+$ cells purified from tasquinimod-treated B16-h5T4 tumors were also less suppressive (Fig. 5B). In this experiment a CFSE-based method was used to detect $CD4^+$ and $CD8^+$ T-cell proliferation. Inhibition of T-cell division by $CD11b^+$ cells was significantly less following tasquinimod treatment. Taken together, these results suggest that tasquinimod modulates not only the infiltration but also the suppressive capacity of tumor-infiltrating myeloid-cell populations.

As shown in figure 4C, the majority of the tumor-infiltrating myeloid cells in the CR Myc-CaP model are macrophages, and tasquinimod treatment reduced $CD206^+$ immunosuppressive M2 macrophages (Fig. 4C and D). This observation led us to investigate the expression of two mechanistically relevant genes, Arg1 (arginase-1) and iNOS (induced nitric oxide synthase) in the tumor-infiltrating myeloid cells (Fig. 5C-E). Previous studies have shown that Arg1 expression is critical to the suppressive function of MDSCs and TAMs. It has been reported that Arg1 gene expression can be regulated by TLR4 pathway [39], which is a target receptor for S100A9. The iNOS marker can be used to differentiate cytotoxic M1 macrophages from immunosuppressive M2 macrophages. Intracellular staining and flow cytometry analysis of CR Myc-CaP tumors showed that tasquinimod reduced arginase-1 expression in myeloid cells, and induced significant iNOS expression, which indicates an increase in immune-promoting M1 macrophages (Fig. 5C). In the B16-5T4 model, mRNA analysis also indicated that tasquinimod shifted an M2 macrophage (immunosuppressive) gene expression signature into an M1 macrophage signature (Fig. 5D). FACS analysis confirmed the reduction of arginase-1 expression and the induction of iNOS in tumor-infiltrating $Ly6C^{high}$ monocytic cells, although not as dramatic as that in the CR Myc-Cap model (Fig.5E).

We also tested the enzymatic activities of nitric oxide synthase and arginase 1 in infiltrating myeloid cells. Tasquinimod treatment *in vivo* led to a significant increase of NOS activity, as compared to vehicle treatment (Supplementary Fig. 6). Arginase activity assay did not reveal a significant change between these two conditions (data not shown).

Tasquinimod treatment reduced the ability of suppressive myeloid cells to support tumor growth

In the therapeutic studies, tasquinimod treatment enhanced immune responses and vaccine effects (Fig. 1 and 2, Supplementary Fig 1). We hypothesize that suppressive myeloid cells, including MDSCs and TAMs and not the other populations, are potential targets of tasquinimod immunomodulatory activity (Fig. 4 and 5, Supplementary Fig. 4 and 5). To test this hypothesis, CR Myc-CaP cells were inoculated into FVB mice as described. When tumor growth was established, mice were randomized into two groups receiving either

vehicle or tasquinimod treatment for 4 weeks. $CD11b^+$ myeloid cells, isolated from tumors that were harvested from different treatment groups, were mixed with fresh CR Myc-CaP cells and inoculated into recipient FVB mice receiving SurVaxM vaccine therapy. As shown in Figure 6, inoculations containing tasquinimod-treated tumor-derived myeloid cells induced significantly slower tumor growth, as compared to those containing vehicle-treated tumor-derived myeloid cells. These data indicate that tasquinimod directly impairs the tumor-promoting activity of immunosuppressive myeloid cells.

Discussion

The aim of immunotherapy is to induce durable and effective immune responses. MDSCs and TAMs contribute to immune tolerance in the tumor microenvironment and consequently affect the efficacy of immunotherapies. Our study provides evidence supporting the development of tasquinimod as a novel approach to target the immunosuppressive TME and facilitate immunotherapy. The data were generated in parallel in two different laboratories, providing evidence for reproducibility of our observations.

We tested two different immunotherapeutic strategies in combination with tasquinimod in two murine tumor models, and observed similar immune promoting effect by tasquinimod coupled to modulation of tumor-infiltrating MDSCs and TAMs. These myeloid populations express receptors for S100A9 and are likely cellular targets for tasquinimod. Furthermore, we demonstrated that the adoptively transferred tasquinimod-treated myeloid cells were sufficient to delay tumor growth in vaccinated animals, as compared to tumor inoculates with vehicle-treated myeloid cells (Fig. 6). There were differences in the subpopulations of tumor-induced myeloid cells in the two models, possibly due to the different tumor origins. Granulocytic MDSCs are prevalent in the CR Myc-CaP model on FVB background, whereas monocytic MDSCs comprise the major population in B16-h5T4 mouse melanoma on C57Bl/6 background. Upon tasquinimod treatment, the $Ly6C^{high}Ly6G^-$ monocytic MDSCs were reduced in the B16-h5T4 tumors (Fig. 4B), and the total $Gr1^+CD11b^+$ MDSCs were reduced in CR Myc-CaP tumors (Fig 4A). At peripheral sites, tasquinimod treatment led to depletion of $Gr1^-CD11b^+$ monocytes in CR Myc-CaP tumor-bearing mice (Supplementary Fig. 2A), and a significant reduction of the $CD11b^+Ly6C^{high}Ly6G^-$ and $CD11b^+Ly6C^{low}Ly6G^-$ monocytic populations in the B16-h5T4 tumor-bearing animals (Supplementary Fig. 3). These observations suggest that immature monocytes are potential targets for tasquinimod. Since monocytic MDSCs or immature monocytes can be precursors of TAMs [38], the reduction of monocytes at peripheral sites could lead to altered profile of TAMs observed in both models (Fig. 4C and D).

As shown in Figure 2C, splenocytes from mice treated with the combined regimen of vaccine and tasquinimod presented increased tumor-cell killing *ex vivo*, compared to that of vehicle and single treatment groups. However, the purified $CD8^+$ effector T cells from mice treated with the combined regimen did not show a significant difference in cytotoxicity against tumor cells. This result suggests that the combined treatment does not affect T effector cell functions directly but instead it relieves the immunosuppression present in the cultures, such as the inhibition by immunosuppressive MDSCs. We observed no inhibition of T-cell proliferation *ex vivo* or when tasquinimod was added to culture at high

concentrations (Supplementary Fig. 4). The effect of combination treatment on specific T-cell activation in tumors was addressed in the B16-h5T4 model. Tracking of superantigen-reactive T cells by TCR-Vβ expression demonstrated increased and prolonged presence of TTS-activated $CD8^+$ T cells in tumors following tasquinimod co-treatment, further supporting the induction of a less immunosuppressive environment. A similar increase in tumor-infiltrating CTLs in B16 tumors was reported recently following TTS therapy in combination with anti-CTLA-4 checkpoint blockade [40].

Previous reports have shown that MDSC-targeting strategies affect systemic or peripheral MDSC accumulation [25] [41]. For example, mAbGB3.1, an antibody against the carboxylated N-glycan on RAGE, reduced MDSC accumulation in blood, spleen and lymph nodes in 4T1 tumor-bearing animals, but not in the metastatic site. However, this antibody treatment did not affect the suppressive function of MDSCs [25]. In our CR Myc-CaP model, tasquinimod did not change the number of $Gr1^+CD11b^+$ MDSCs at peripheral sites (Supplementary Fig. 2), which would suggest that tasquinimod does not affect the generation or expansion of MDSCs. However, tasquinimod reduced tumor-infiltrating MDSCs (Fig. 4A). This observation suggests that tasquinimod may inhibit MDSC trafficking/accumulation in the tumor, leading to modulation of the TME and relief of immune tolerance. In support of this finding, S100A9 signaling has been reported to regulate both expansion and migration of MDSCs [24-25]. It has also been shown that intracellular S100A9 expression in myeloid progenitor cells induces MDSC expansion [24] [42]. However, extracellular (secreted) S100A9 protein binds to carboxylated N-glycan receptors (RAGE) that are expressed on the surface of MDSCs and promotes MDSC migration to the site of tumors [25, 43]. Taken together, our results provide evidence supporting a mechanism of action by tasquinimod in blocking extracellular S100A9 and receptor signaling that may be critical to MDSC tumor infiltration, via cell surface receptors such as TLR4 [23] and RAGE [22].

The notion of a cross-talk between different regulatory myeloid cells is well established [44]. Besides the reduction and modulation of tumor-associated MDSCs, tasquinimod treatment resulted in decreased numbers of $CD206^+$ M2-polarized TAMs and reduced the suppressive function of CD11b-expressing myeloid infiltrates (Fig. 4 and 5). Macrophages are categorized as either the classically activated, cytotoxic M1 macrophages or the alternatively activated, suppressive M2 macrophages. The M2-polarized TAMs are enriched in hypoxic tumor areas with a superior pro-angiogenic activity *in vivo*, a limited capacity to present antigen, and the ability to suppress adaptive immune responses such as T-cell activation [38, 45]. In the CR Myc-CaP and B16-5T4 models, $F4/80^+$ macrophages represent the major population of tumor infiltrates and a large component of these infiltrating macrophages are $CD206^+$, M2-like type, which is significantly reduced upon tasquinimod treatment (Fig. 4C and D). The function of macrophages depends on the expression of arginase-1 and iNOS. While classically activated M1-polarized macrophages express both arginase-1 and iNOS, suppressive TAMs only express arginase-1, which is critical for the immunosuppressive function. As shown in Figure 5, tasquinimod treatment reduced arginase-1 expression in $CD11b^+$ cells in both models (Fig. 5C-E), which could explain the reduced suppressive function of these cells (Fig. 5A and B). An important

regulator of arginase-1 gene expression is TLR4 signaling [39], which is a receptor for a tasquinimod-target protein, S100A9. Potentially, the S100A9-TLR4-arginase 1 pathway may be involved in tasquinimod-induced changes of suppressive myeloid cells. Interestingly, in the CR Myc-CaP model, tasquinimod induced iNOS expression in $CD11b^+$ cells (Fig. 5C). An assay testing NOS enzyme also showed that tasquinimod-treated CD11b cells had higher NOS activity (Supplementary Fig. 6). iNOS is mainly expressed in macrophages and monocytic MDSCs, whereas granulocytic MDSCs have low iNOS. Therefore, the increase of iNOS in CD11b cells is likely due to an increase of M1 macrophages in the tumor, rather than an induction of monocytic MDSCs since the vast majority of MDSCs in the tumors of this model is of the granulocytic type (Supplementary Fig. 2D).

Tasquinimod has pleiotropic effects that contribute to its antitumor activity, including anti-angiogenesis, immunomodulation, and inhibition of metastasis. As demonstrated in this study, modulation of suppressive myeloid cells may represent a critical biologic mechanism of action of tasquinimod and the common target giving rise to the diverse effects. Immunosuppressive myeloid cells (MDSCs and TAMs) secret multiple factors, including VEGF and MMP9, that promote angiogenesis [46]. In a hypoxic microenvironment myeloid cells can also recruit endothelial cells and their precursors [47]. MDSCs have also been reported to promote tumor-cell dissemination [48] and cancer stemness [49]. In addition, MDSCs and TAMs have potential to prime distal sites to promote the seeding of metastatic tumor cells [50-52]. Moreover, MDSCs have been found to promote cancer cell survival upon chemotherapy by producing certain chemokines [53]. These evidences suggest that suppressive myeloid populations represent key mediators of multiple critical aspects of cancer immune tolerance, metastasis and drug resistance. The inhibitory effects of tasquinimod on tumor-infiltrating immunosuppressive myeloid cells, and, in particular, on the M2-polarized TAMs, have been observed in pre-clinical syngeneic tumor models. These biological properties of tasquinimod support the further development of this agent for clinical combination strategies with immunotherapies such as vaccines and immune checkpoint inhibitors. Based on our preliminary data, a clinical trial of tasquinimod in combination with sipuleucel-T in patients with metastatic castration-resistant prostate cancer is planned to open in 2014.

In conclusion, tasquinimod is a small molecule inhibitor with a potentially unique mechanism of action that targets the tumor microenvironment. Future preclinical and clinical testing of this agent will define its application in a wide range of therapeutic strategies including immunotherapies, anti-angiogenic and anti-metastatic drugs.

Supplementary Material

Refer to Web version on PubMed Central for supplementary material.

Acknowledgments

We thank Anneli Nilsson, Jan Nilsson, Therese Blidberg and Martin Stenström for excellent technical assistance and Dr. Lennart Ohlsson (MicroMorph Histology Services, Lund, Sweden) for performing immunohistochemistry.

FUNDING

National Cancer Institute- P50 CA58236 (R.P.)

References

1. Small EJ, Schellhammer PF, Higano CS, Redfern CH, Nemunaitis JJ, Valone FH, et al. Placebo-controlled phase III trial of immunologic therapy with sipuleucel-T (APC8015) in patients with metastatic, asymptomatic hormone refractory prostate cancer. J Clin Oncol. 2006; 24:3089–94. [PubMed: 16809734]
2. Smith JL Jr, Stehlin JS Jr. Spontaneous regression of primary malignant melanomas with regional metastases. Cancer. 1965; 18:1399–415. [PubMed: 5844157]
3. Culver ME, Gatesman ML, Mancl EE, Lowe DK. Ipilimumab: a novel treatment for metastatic melanoma. Ann Pharmacother. 2011; 45:510–9. [PubMed: 21505108]
4. Gabrilovich DI, Nagaraj S. Myeloid-derived suppressor cells as regulators of the immune system. Nat Rev Immunol. 2009; 9:162–74. [PubMed: 19197294]
5. Oosterling SJ, van der Bij GJ, Meijer GA, Tuk CW, van Garderen E, van Rooijen N, et al. Macrophages direct tumour histology and clinical outcome in a colon cancer model. J Pathol. 2005; 207:147–55. [PubMed: 16104052]
6. Pan PY, Wang GX, Yin B, Ozao J, Ku T, Divino CM, Chen SH. Reversion of immune tolerance in advanced malignancy: modulation of myeloid-derived suppressor cell development by blockade of stem-cell factor function. Blood. 2008; 111:219–28. [PubMed: 17885078]
7. Sinha P, Clements VK, Fulton AM, Ostrand-Rosenberg S. Prostaglandin E2 promotes tumor progression by inducing myeloid-derived suppressor cells. Cancer Res. 2007; 67:4507–13. [PubMed: 17483367]
8. Song X, Krelin Y, Dvorkin T, Bjorkdahl O, Segal S, Dinarello CA, et al. CD11b+/Gr-1+ immature myeloid cells mediate suppression of T cells in mice bearing tumors of IL-1beta-secreting cells. J Immunol. 2005; 175:8200–8. [PubMed: 16339559]
9. Solito S, Bronte V, Mandruzzato S. Antigen specificity of immune suppression by myeloid-derived suppressor cells. J Leukoc Biol. 2011; 90:31–6. [PubMed: 21486906]
10. Huang B, Pan PY, Li Q, Sato AI, Levy DE, Bromberg J, et al. Gr-1+CD115+ immature myeloid suppressor cells mediate the development of tumor-induced T regulatory cells and T-cell anergy in tumor-bearing host. Cancer Res. 2006; 66:1123–31. [PubMed: 16424049]
11. Serafini P, Mgebroff S, Noonan K, Borrello I. Myeloid-derived suppressor cells promote cross-tolerance in B-cell lymphoma by expanding regulatory T cells. Cancer Res. 2008; 68:5439–49. [PubMed: 18593947]
12. Yang Z, Zhang B, Li D, Lv M, Huang C, Shen GX, Huang B. Mast cells mobilize myeloid-derived suppressor cells and Treg cells in tumor microenvironment via IL-17 pathway in murine hepatocarcinoma model. PLoS One. 2010; 5:e8922. [PubMed: 20111717]
13. Mills CD, Kincaid K, Alt JM, Heilman MJ, Hill AM. M-1/M-2 macrophages and the Th1/Th2 paradigm. J Immunol. 2000; 164:6166–73. [PubMed: 10843666]
14. Pili R, Häggman M, Stadler WM, Gingrich JR, Assikis VJ, Björk A, et al. Phase II randomized, double-blind, placebo-controlled study of tasquinimod in men with minimally symptomatic metastatic castrate-resistant prostate cancer. J Clin Oncol. 2011; 29:4022–8. [PubMed: 21931019]
15. Armstrong AJ, Häggman M, Stadler WM, Gingrich JR, Assikis V, Polikoff J, et al. Long-term Survival and Biomarker Correlates of Tasquinimod Efficacy in a Multicenter Randomized Study of Men with Minimally Symptomatic Metastatic Castration-Resistant Prostate Cancer. Clin Cancer Res. 2013; 19:6891–901. [PubMed: 24255071]
16. Dalrymple SL, Becker RE, Isaacs JT. The quinoline-3-carboxamide anti-angiogenic agent, tasquinimod, enhances the anti-prostate cancer efficacy of androgen ablation and taxotere without effecting serum PSA directly in human xenografts. Prostate. 2007; 67:790–7. [PubMed: 17373719]

17. Dalrymple SL, Becker RE, Zhou H, DeWeese TL, Isaacs JT. Tasquinimod prevents the angiogenic rebound induced by fractionated radiation resulting in an enhanced therapeutic response of prostate cancer xenografts. Prostate. 2012; 72:638–48. [PubMed: 21837778]
18. Jennbacken K, Welén K, Olsson A, Axelsson B, Törngren M, Damber JE, Leanderson T. Inhibition of metastasis in a castration resistant prostate cancer model by the quinoline-3-carboxamide tasquinimod (ABR-215050). Prostate. 2012; 72:913–24. [PubMed: 22287276]
19. Isaacs JT, Pili R, Qian DZ, Dalrymple SL, Garrison JB, Kyprianou N, et al. Identification of ABR-215050 as lead second generation quinoline-3-carboxamide anti-angiogenic agent for the treatment of prostate cancer. Prostate. 2006; 66:1768–78. [PubMed: 16955399]
20. Olsson A, Björk A, Vallon-Christersson J, Isaacs JT, Leanderson T. Tasquinimod (ABR-215050), a quinoline-3-carboxamide anti-angiogenic agent, modulates the expression of thrombospondin-1 in human prostate tumors. Mol Cancer. 2010; 9:107. [PubMed: 20470445]
21. Isaacs JT, Antony L, Dalrymple SL, Brennen WN, Gerber S, Hammers H, et al. Tasquinimod Is an Allosteric Modulator of HDAC4 survival signaling within the compromised cancer microenvironment. Cancer Res. 2013; 73:1386–99. [PubMed: 23149916]
22. Bjork P, Björk A, Vogl T, Stenström M, Liberg D, Olsson A, et al. Identification of human S100A9 as a novel target for treatment of autoimmune disease via binding to quinoline-3-carboxamides. PLoS Biol. 2009; 7:e97. [PubMed: 19402754]
23. Kallberg E, Vogl T, Liberg D, Olsson A, Björk P, Wikström P, et al. S100A9 interaction with TLR4 promotes tumor growth. PLoS One. 2012; 7:e34207. [PubMed: 22470535]
24. Cheng P, Corzo CA, Luetteke N, Yu B, Nagaraj S, Bui MM, et al. Inhibition of dendritic cell differentiation and accumulation of myeloid-derived suppressor cells in cancer is regulated by S100A9 protein. J Exp Med. 2008; 205:2235–49. [PubMed: 18809714]
25. Sinha P, Okoro C, Foell D, Freeze HH, Ostrand-Rosenberg S, Srikrishna G. Proinflammatory S100 proteins regulate the accumulation of myeloid-derived suppressor cells. J Immunol. 2008; 181:4666–75. [PubMed: 18802069]
26. Ellis L, Lehet K, Ramakrishnan S, Adelaiye R, Pili R. Development of a castrate resistant transplant tumor model of prostate cancer. Prostate. 2011; 72:587–91. [PubMed: 21796655]
27. Mulryan K, Ryan MG, Myers KA, Shaw D, Wang W, Kingsman SM, et al. Attenuated recombinant vaccinia virus expressing oncofetal antigen (tumor-associated antigen) 5T4 induces active therapy of established tumors. Mol Cancer Ther. 2002; 1:1129–37. [PubMed: 12481437]
28. Attia MA, Weiss DW. Immunology of spontaneous mammary carcinomas in mice. V. Acquired tumor resistance and enhancement in strain A mice infected with mammary tumor virus. Cancer Res. 1966; 26:1787–800. [PubMed: 4288553]
29. Kishi H, Igawa M, Kikuno N, Yoshino T, Urakami S, Shiina H. Expression of the survivin gene in prostate cancer: correlation with clinicopathological characteristics, proliferative activity and apoptosis. J Urol. 2004; 171:1855–60. [PubMed: 15076293]
30. Ciesielski MJ, Ahluwalia MS, Munich SA, Orton M, Barone T, Chanan-Khan A, Fenstermaker RA. Antitumor cytotoxic T-cell response induced by a survivin peptide mimic. Cancer Immunol Immunother. 2010; 59:1211–21. [PubMed: 20422411]
31. Shen L, Ciesielski M, Ramakrishnan S, Miles KM, Ellis L, Sotomayor P, et al. Class I histone deacetylase inhibitor entinostat suppresses regulatory T cells and enhances immunotherapies in renal and prostate cancer models. PLoS One. 2012; 7:e30815. [PubMed: 22303460]
32. Dohlsten M, Abrahmsén L, Björk P, Lando PA, Hedlund G, Forsberg G, Brodin T, et al. Monoclonal antibody-superantigen fusion proteins: tumor-specific agents for T-cell-based tumor therapy. Proc Natl Acad Sci U S A. 1994; 91:8945–9. [PubMed: 8090750]
33. Kappler J, Kotzin B, Herron L, Gelfand EW, Bigler RD, Boylston A, et al. V beta-specific stimulation of human T cells by staphylococcal toxins. Science. 1989; 244:811–3. [PubMed: 2524876]
34. Raymond E, Dalgleish A, Damber JE, Smith M, Pili R. Mechanisms of action of tasquinimod on the tumour microenvironment. Cancer Chemother Pharmacol. 2014; 73:1–8. [PubMed: 24162378]
35. De Palma M, Venneri MA, Galli R, Sergi Sergi L, Politi LS, Sampaolesi M, Naldini L. Tie2 identifies a hematopoietic lineage of proangiogenic monocytes required for tumor vessel formation

and a mesenchymal population of pericyte progenitors. Cancer Cell. 2005; 8:211–26. [PubMed: 16169466]

36. Sica A, Bronte V. Altered macrophage differentiation and immune dysfunction in tumor development. J Clin Invest. 2007; 117:1155–66. [PubMed: 17476345]
37. Peranzoni E, Zilio S, Marigo I, Dolcetti L, Zanovello P, Mandruzzato S, Bronte V. Myeloid-derived suppressor cell heterogeneity and subset definition. Curr Opin Immunol. 2010; 22:238–44. [PubMed: 20171075]
38. Movahedi K, Guilliams M, Van den Bossche J, Van den Bergh R, Gysemans C, Beschin A, et al. Identification of discrete tumor-induced myeloid-derived suppressor cell subpopulations with distinct T cell-suppressive activity. Blood. 2008; 111:4233–44. [PubMed: 18272812]
39. El Kasmi KC, Qualls JE, Pesce JT, Smith AM, Thompson RW, Henao-Tamayo M, et al. Toll-like receptor-induced arginase 1 in macrophages thwarts effective immunity against intracellular pathogens. Nat Immunol. 2008; 9:1399–406. [PubMed: 18978793]
40. Sundstedt A, Celander M, Eriksson H, Törngren M, Hedlund G. Monotherapeutically nonactive CTLA-4 blockade results in greatly enhanced antitumor effects when combined with tumor-targeted superantigens in a B16 melanoma model. J Immunother. 2012; 35:344–53. [PubMed: 22495392]
41. Rigamonti N, Capuano G, Ricupito A, Jachetti E, Grioni M, Generoso L, et al. Modulators of arginine metabolism do not impact on peripheral T-cell tolerance and disease progression in a model of spontaneous prostate cancer. Clin Cancer Res. 2011; 17:1012–23. [PubMed: 21248302]
42. Chen X, Eksioglu EA, Zhou J, Zhang L, Djeu J, Fortenbery N, et al. Induction of myelodysplasia by myeloid-derived suppressor cells. J Clin Invest. 2013; 123:4595–611. [PubMed: 24216507]
43. Ichikawa M, Williams R, Wang L, Vogl T, Srikrishna G. S100A8/A9 activate key genes and pathways in colon tumor progression. Mol Cancer Res. 2011; 9:133–48. [PubMed: 21228116]
44. Ostrand-Rosenberg S, Sinha P, Beury DW, Clements VK. Cross-talk between myeloid-derived suppressor cells (MDSC), macrophages, and dendritic cells enhances tumor-induced immune suppression. Semin Cancer Biol. 2012; 22:275–81. [PubMed: 22313874]
45. De Palma M, Lewis CE. Macrophage regulation of tumor responses to anticancer therapies. Cancer Cell. 2013; 23:277–86. [PubMed: 23518347]
46. Murdoch C, Muthana M, Coffelt SB, Lewis CE. The role of myeloid cells in the promotion of tumour angiogenesis. Nat Rev Cancer. 2008; 8:618–31. [PubMed: 18633355]
47. Li B, Vincent A, Cates J, Brantley-Sieders DM, Polk DB, Young PP. Low levels of tumor necrosis factor alpha increase tumor growth by inducing an endothelial phenotype of monocytes recruited to the tumor site. Cancer Res. 2009; 69:338–48. [PubMed: 19118019]
48. Toh B, Wang X, Keeble J, Sim WJ, Khoo K, Wong WC, et al. Mesenchymal transition and dissemination of cancer cells is driven by myeloid-derived suppressor cells infiltrating the primary tumor. PLoS Biol. 2011; 9:e1001162. [PubMed: 21980263]
49. Cui TX, Kryczek I, Zhao L, Zhao E, Kuick R, Roh MH, et al. Myeloid-derived suppressor cells enhance stemness of cancer cells by inducing microRNA101 and suppressing the corepressor CtBP2. Immunity. 2013; 39:611–21. [PubMed: 24012420]
50. Hiratsuka S, Watanabe A, Aburatani H, Maru Y. Tumour-mediated upregulation of chemoattractants and recruitment of myeloid cells predetermines lung metastasis. Nat Cell Biol. 2006; 8:1369–75. [PubMed: 17128264]
51. Sawant A, Deshane J, Jules J, Lee CM, Harris BA, Feng X, Ponnazhagan S. Myeloid-derived suppressor cells function as novel osteoclast progenitors enhancing bone loss in breast cancer. Cancer Res. 2013; 73:672–82. [PubMed: 23243021]
52. Kaplan RN, Riba RD, Zacharoulis S, Bramley AH, Vincent L, Costa C, et al. VEGFR1-positive haematopoietic bone marrow progenitors initiate the pre-metastatic niche. Nature. 2005; 438:820–7. [PubMed: 16341007]
53. Acharyya S, Oskarsson T, Vanharanta S, Malladi S, Kim J, Morris PG, et al. A CXCL1 paracrine network links cancer chemoresistance and metastasis. Cell. 2012; 150:165–78. [PubMed: 22770218]

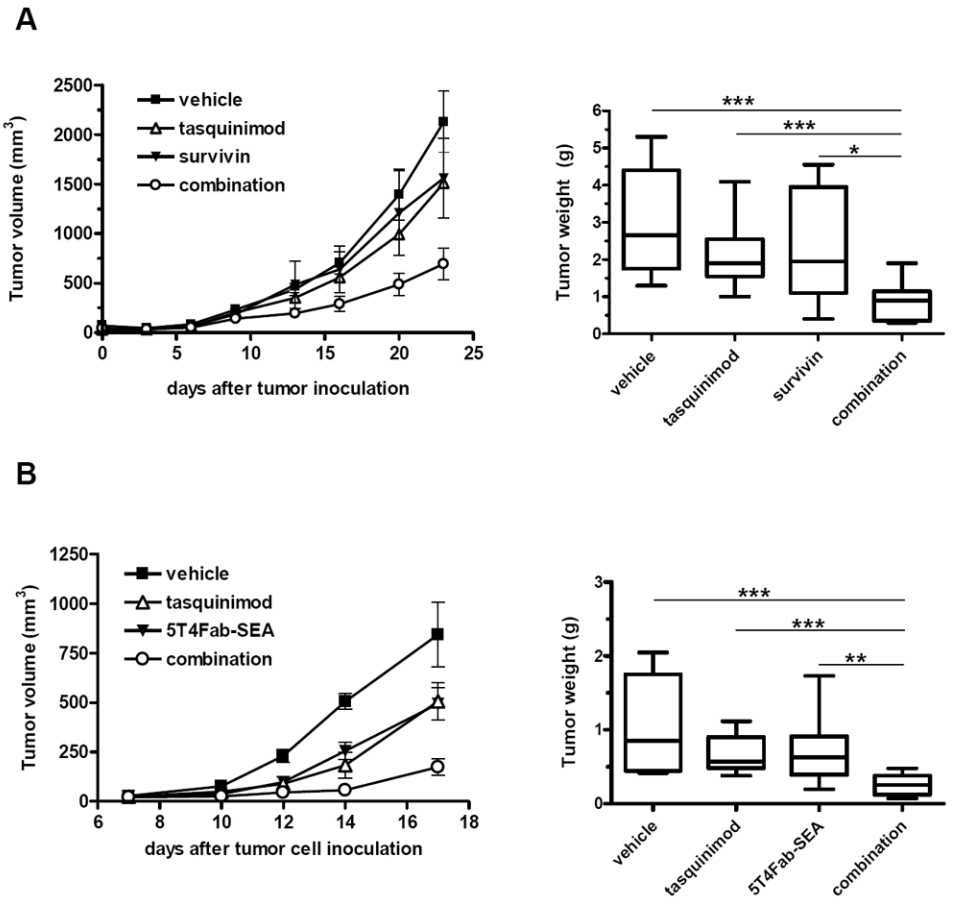

Figure 1. Tasquinimod improves immunotherapy in CR Myc-CaP prostate cancer and B16 melanoma models

A. Mice were inoculated s.c. with CR Myc-CaP cells. When the tumors reached an average size of 25 mm^2, mice were treated with vehicle, survivin, tasquinimod or the combination of survivin and tasquinimod. Left panel shows tumor growth curves by serial caliper measurements. Right panel shows tumor weights at the endpoint. **B**. Mice were inoculated s.c. with B16-h5T4 cells and treatment with tasquinimod was initiated the day after inoculation and continued throughout the experiment. The TTS protein 5T4Fab-SEA (25μg/kg) was given as daily i.v. injections on days 3 to 6. Left panel shows tumor growth curves by serial caliper measurements. Right panel shows end of treatment tumor weights. The experiments were repeated at least twice. Results from one representative experiment are shown. (* $p<0.05$; ** $p<0.01$; *** $p<0.001$; Mann-Whitney U. Error bars indicate s.e.m.)

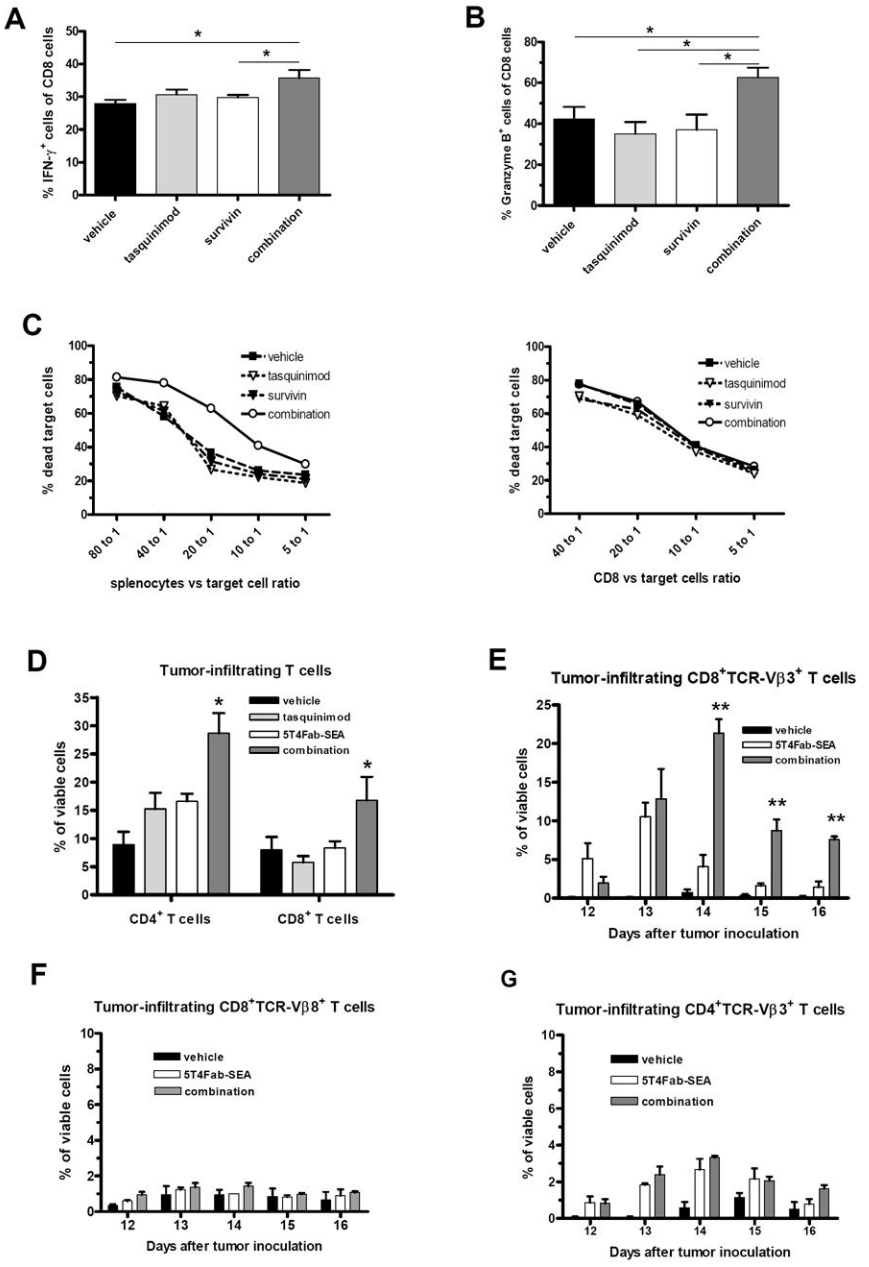

Figure 2. Tasquinimod in combination with vaccine or TTS improves T-cell immune responses

Splenocytes isolated from CR Myc-CaP tumor-bearing mice were stimulated with **A**. PMA and Ionomycin for 5 hours in the presence of BFA for IFNγ production, or **B**. on CD3- and CD28-coated plates for 72 hours for Granzyme B production (BFA was added during the last 5 hours). **C**. Splenocytes (left panel) or purified $CD8^+$ T cells (right panel) from CR Myc-CaP tumor-bearing mice were co-cultured with DIO-labeled tumor cells in different ratios for 5 hours. Propidium iodide was added at the end of incubation to detect tumor cell death. **D**. FACS analysis of tumor-infiltrating T cells performed at the endpoint of the experiment depicted in Fig. 1B. **E-G**. FACS analysis of infiltrating T cells in B16-h5T4

tumors at different time points. 5T4Fab-SEA was administered on days 9-11. (*$p < 0.05$; **$p < 0.01$; ***p<0.001, t-test. Error bars indicate s.e.m.)

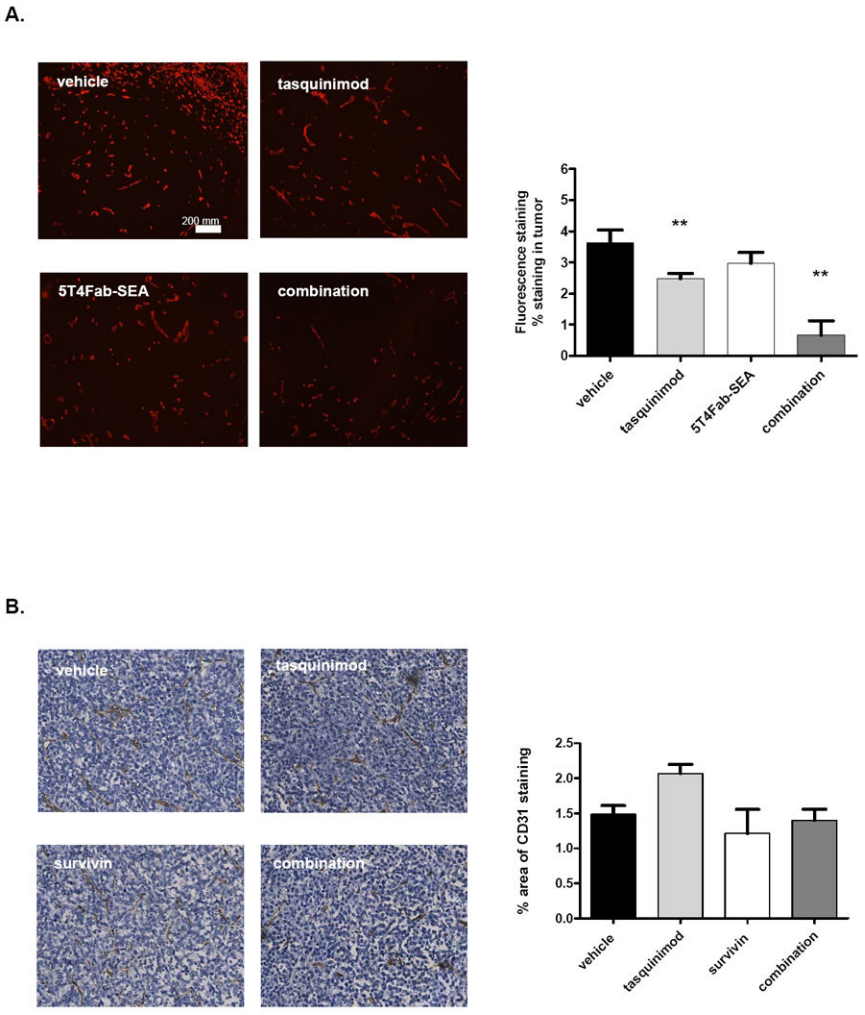

Figure 3. Tasquinimod effects on tumor vasculature (CD31) in B16-h5T4 and CR Myc-CaP tumors

A. Immunofluorescence staining of $CD31^+$ vasculature in B16-h5T4 tumors. **B**. Immunohistochemistry staining of $CD31^+$ vasculature in CR Myc-CaP tumors. The experiments were repeated at least twice. Results from one representative experiment are shown. (**$p < 0.01$; t-test. Error bars indicate s.e.m.)

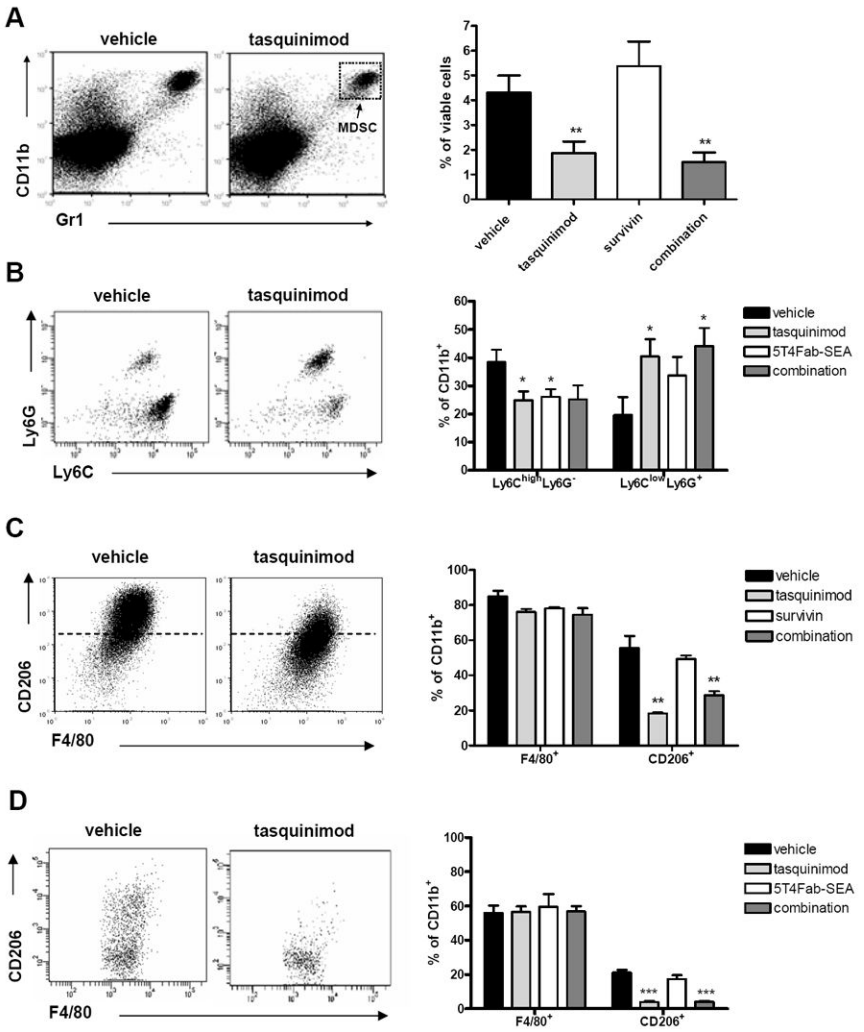

Figure 4. Tasquinimod modulates MDSC populations in the CR Myc-CaP and B16-h5T4 tumor models

A. FACS analysis of tumor-cell suspensions from the CR Myc-CaP model for $CD11b^{+}Gr1^{+}$ MDSCs after tasquinimod treatment. **B**. FACS analysis of tumor-cell suspensions from the B16-h5T4 model for granulocytic $Ly6G^{+}Ly6C^{low}$ and monocytic $Ly6G^{-}Ly6C^{high}$ $GR1^{+}$ MDSCs. FACS analysis of tumor-cell suspensions for $F4/80^{+}$ macrophages and for CD206 expression from (**C.)** CR Myc-CaP tumors; and (**D**.) B16-5T4 tumors. FACS plots and quantifications are depicted throughout. (*$p < 0.05$; ** = $p<0.01$; *** $p<0.001$, t-test. Error bars indicate s.e.m.)

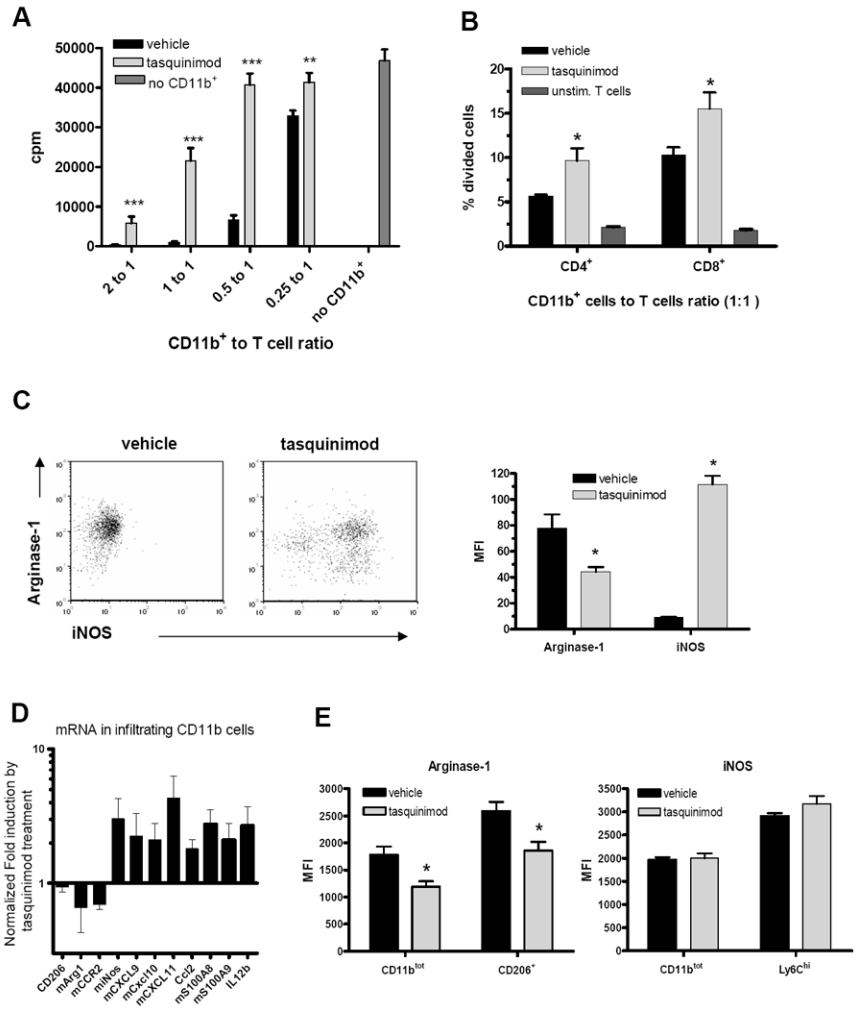

Figure 5. Tasquinimod treatment reduces the suppressive capacity of tumor-infiltrating CD11b$^+$ cells in the CR Myc-CaP and B16-h5T4 tumor models

A. CD11b$^+$ cells were enriched from CR Myc-CaP tumors, and added at different ratios to stimulated T-cell cultures. ^{3}[H]-thymidine was added to the cultures during the last 12 hours of 3-days culturing. **B**. CD11b$^+$ cells were purified from B16-h5T4 tumors and co-cultured with purified CFSE-labeled T cells for 3 days. The frequencies of divided cells among CD4$^+$ and CD8$^+$ T cells were measured by FACS. **C**. Intracellular staining of arginase-1 and iNOS in infiltrating CD11b$^+$ cells from CR Myc-CaP tumors. **D**. qRT-PCR analyses of selected genes expressed in purified CD11b$^+$ cells from B16-h5T4 tumors. **E**. Intracellular staining of arginase-1 and iNOS in infiltrating CD11b$^+$ cells isolated from B16h5T4 tumors. (*p < 0.05; **p < 0.01; ***p<0.001, t-test. Error bars indicate s.e.m.)

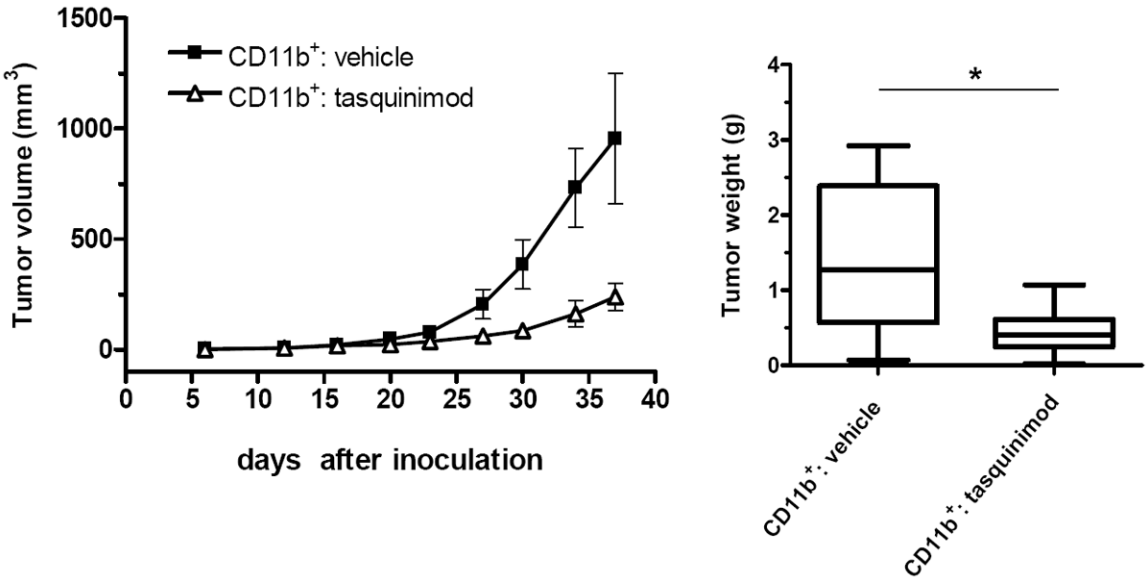

Figure 6. Tasquinimod treatment reduces the ability of suppressive myeloid cells to support tumor growth

$CD11b^+$ cells were isolated from tumors collected from either vehicle or tasquinimod-treated donor mice, mixed with fresh CR Myc-CaP cells (mixture contained 1.5×10^6 CR Myc-CaP cells and 0.75×10^6 CD11b cells), and inoculated s.c. into recipient mice receiving SurVaxM vaccine. Recipient mice received two doses of the vaccine before inoculation and two additional doses were administered after tumor-cell inoculation. Left panel shows tumor growth curves by serial caliper measurements. Right panel shows end of treatment tumor weights. (*$p < 0.05$, t-test. Error bars indicate s.e.m.)